Crystalline Morphology and Isothermal Crystallization Kinetics of Poly(ethylene terephthalate)/Clay Nanocomposites

Tong Wan, Ling Chen, Yang Choo Chua, Xuehong Lu

School of Materials Engineering, Nanyang Technology University, Nanyang Avenue, Singapore 639798

Received 26 November 2003; accepted 27 April 2004
DOI 10.1002/app.20975
Published online in Wiley InterScience (www.interscience.wiley.com).

ABSTRACT: A poly(ethylene terephthalate) (PET)/montmorillonite clay nanocomposite was synthesized via *in situ* polymerization. Microscopic studies revealed that in an isothermal crystallization process, some crystallites in the nanocomposite initially were rod-shaped and later exhibited three-dimensional growth. The crystallites in the nanocomposite were irregularly shaped, rather than spherulitic, being interlocked together without clear boundaries, and they were much smaller than those of neat PET. With Avrami analysis, the isothermal crystallization kinetic parameters (the Avrami exponent and constant) were obtained. The rate constants for the nanocomposite demonstrated that clay could greatly increase the crystallization rate of PET. The results for the Avrami exponent were consistent with the observation of the rodlike crystallites in the PET/clay nanocomposite during the initial stage. Wide-angle X-ray scattering and Fourier transform infrared studies showed that, in comparison with neat PET, the crystal lattice parameters and crystallinity of the nanocomposite did not change significantly, whereas more defects may have been present in the crystalline regions of the nanocomposite because of the presence of the clay. J Appl Polym Sci 94: 1381–1388, 2004

Key words: clay; morphology; nanocomposites

INTRODUCTION

It is well known that polymer/clay nanocomposites can exhibit significant improvements in thermomechanical and gas barrier properties over their neat polymer counterparts at relatively low clay loadings. The key to the unique behaviors and exceptional properties exhibited by polymer/clay nanocomposites is the dispersion of the clay into nanometer-thick layers within the polymer matrices. The presence of nanometer-sized clay layers in a semicrystalline polymer matrix not only creates an enormous interfacial area but also greatly affects the crystallization behavior of the matrix. A number of recent works have shown that the addition of clay to a semicrystalline polymer, such as nylon 6 or polypropylene, on a nanometer scale may significantly change the crystal form, size, and morphology and increase the crystallization rate of the polymer;[1–5] this inevitably has an impact on the properties of the material.

Poly(ethylene terephthalate) (PET) is a widely used high-performance polymer. The preparation of PET/clay nanocomposites has been attempted by several groups. Because it is difficult to achieve an exfoliated structure with clay in PET and PET has a very slow crystallization rate, studies performed on PET/clay nanocomposites so far have mainly been concerned with improving the dispersion of clay in PET[6–8] and establishing whether clay can heterogeneously nucleate the crystallization of the PET matrix [8,9] The effects of clay on the crystalline morphology of PET/clay nanocomposites have not been addressed. This article focuses on isothermal crystallization and the resultant crystalline morphology of a PET/clay nanocomposite. During an isothermal crystallization process, some crystallites in the nanocomposite initially are rod-shaped and later exhibit three-dimensional growth. The crystallites in the nanocomposite are irregularly shaped, rather than spherulitic, and are much smaller than those of neat PET. These unique crystalline morphological features of the nanocomposite may have a significant impact on its properties, especially its mechanical properties. Although this article describes the crystalline morphology and its development in a PET/clay nanocomposite, the knowledge gained here could be of considerable general interest for the study of semicrystalline polymer nanocomposites.

EXPERIMENTAL

Materials

A PET/clay nanocomposite containing 3 wt % montmorillonite clay was synthesized via the polymeriza-

Correspondence to: X. Lu (asxhlu@ntu.edu.sg).

tion of bis(2-hydroxyethyl) terephthalate (BHET) in the presence of an organoclay modified with 12-aminododecanoic acid.[10,11] Manganese(II) acetate (MnAc) and antimony(III) trioxide (Sb_2O_3) were used as catalysts, and triphenyl phosphate (TPP) was used as a stabilizer. The unmodified montmorillonite clay was supplied by Nanocor, Inc. (Arlington Heights, IL) and the other chemicals were purchased from Aldrich (Milwaukee, WI) without further treatment. BHET and the clay were mixed in a flask, and the mixture was first kept at 120°C for 30 min under nitrogen. The temperature was then increased to 190°C and kept at 190°C for another 30 min in the presence of MnAc and TPP. The temperature was further increased to 290°C, and a vacuum (<1 mbar) was applied in the presence of Sb_2O_3; the temperature and vacuum were maintained for 1 h. Mechanical stirring was applied throughout the polymerization process. Neat PET was synthesized with the same procedure as a reference. The intrinsic viscosities of the neat PET and the PET/clay nanocomposite were 0.62 and 0.59 g/dL, respectively, as measured at 25°C in a 1,1,2,2-tetrachloroethane/phenol mixture (50/50 w/w).

Wide-angle X-ray scattering (WAXS)

The *d*-spacings of clay layers in the raw and modified clay and the nanocomposite were measured with a Rigaku X-ray diffractometer (Tokyo, Japan) with Cu Kα radiation. WAXS measurements were also conducted on neat PET, and the nanocomposite samples were isothermally crystallized at 226°C for 1 h. All the samples were scanned at a rate of 1°/min and in a 2θ range of 1–60°.

Transmission electron microscopy (TEM)

A Leica Ultracut UCT ultramicrotome (Vienna, Austria) was used to section the PET/clay nanocomposite into thin slices. After the sectioning, the ultrathin sections were collected on 200-mesh copper grids. A JEOL 2010 TEM instrument (Tokyo, Japan) was used to examine the sections to observe the clay distribution in the PET matrix.

Polarizing optical microscopy (POM)

A Nikon Optiphot-Pol universal stage polarizing optical microscope (Tokyo, Japan) was used to examine the clay particle size in the PET/clay nanocomposite and to observe the isothermal crystallization processes of neat PET and the nanocomposite. A thin sample piece weighing about 5 mg was sandwiched between two glass coverslips and placed on a digital hotplate under nitrogen. The hotplate was rapidly heated to 330°C and kept at 330°C for 3 min to ensure the complete melting of the PET crystallites. The melt was gently pressed to achieve a uniform thickness of about 0.1 mm. For the examination of the clay particle size, the nanocomposite melt was cooled to 300°C and kept at this temperature for observation. For the study of the PET crystalline morphology, neat PET and nanocomposite melts were rapidly cooled to the crystallization temperature of 226°C and kept at this temperature for observation. All the observations were made under crossed polarizers. A CCD camera was used to snap the optical texture images.

Scanning electron microscopy (SEM)

Neat PET and the nanocomposite were made into flat discs by complete melting on a hot stage followed by compression. They were then isothermally crystallized at 226°C for 30 min under nitrogen and chemically etched with a potassium hydroxide/methanol (5/95 w/w) solution and *N*-propylamine.[12,13] The etched samples were coated with gold and then observed under a JEOL JSM-5410 scanning electron microscope (Tokyo, Japan) with a working voltage of 10 kV.

Differential scanning calorimetry (DSC)

Isothermal crystallization was carried out in a cell of a TA Instruments 2920 MDSC instrument at various temperatures ranging from 210 to 230°C at a nitrogen flow rate of 50 cc/min. Before the isothermal processes, in the cell the samples were rapidly heated to 300°C and cooled to the crystallization temperature. The heat flow was recorded as a function of time until the heat-flow curve returned to the calorimeter baseline.

Fourier transform infrared (FTIR) spectroscopy

Infrared spectra of neat PET and the nanocomposite were recorded with a PerkinElmer 2000 FTIR instru-

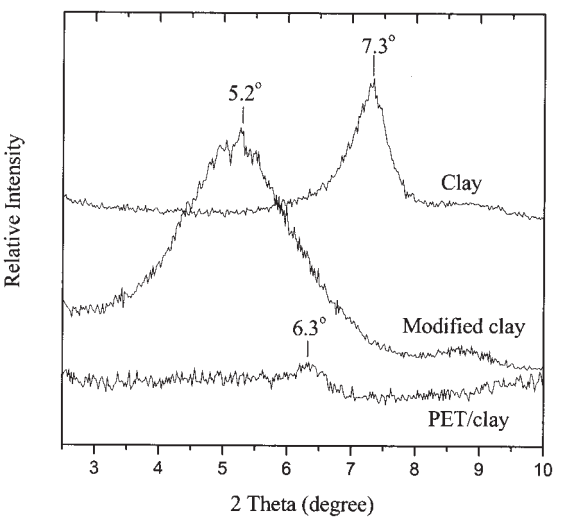

Figure 1 WAXS patterns of the raw and modified clay and the clay in the PET/clay nanocomposite.

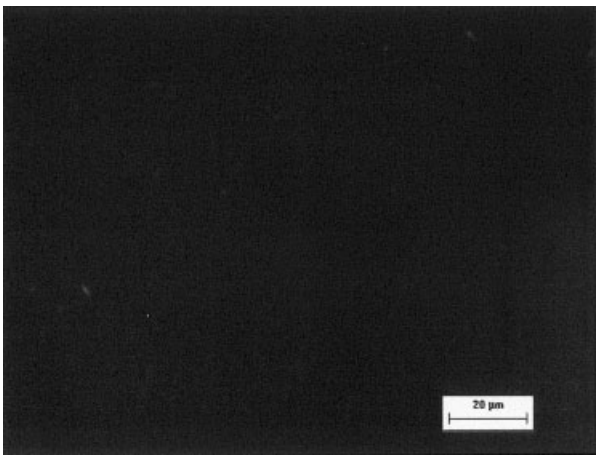

Figure 2 POM picture of the PET/clay nanocomposite at 300°C under crossed polarizers. The micrometer-sized clay particles can scarcely be observed (bar = 20 μm).

ment (Norwalk, CT). Each sample was scanned 100 times at a resolution of 2 cm^{-1} from 1200 to 800 cm^{-1}. Before the FTIR measurements, the samples were isothermally crystallized at 226°C for 1 h under nitrogen.

RESULTS AND DISCUSSION

Dispersion of the clay in the PET matrix

Figure 1 shows the WAXS patterns of the raw and modified clay and the clay in the PET/clay nanocom-

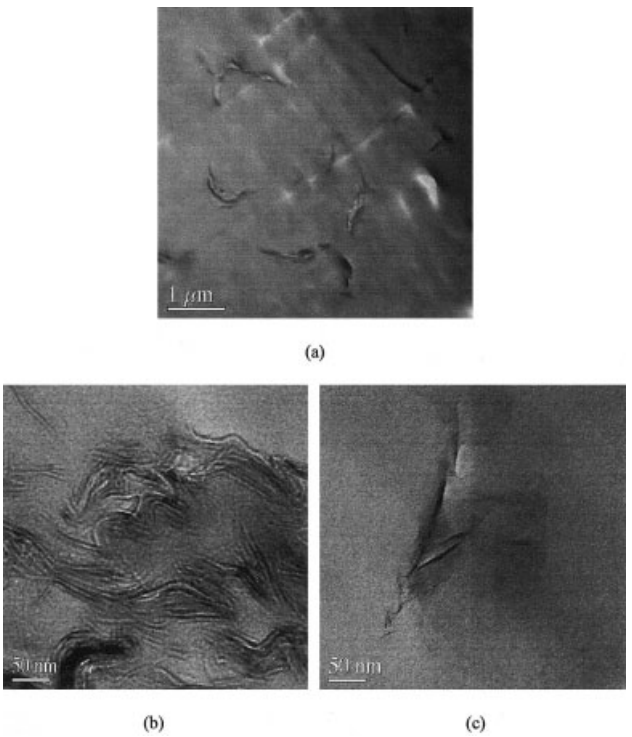

Figure 3 TEM pictures of the PET/clay nanocomposite showing (a) agglomerates of clay particles, (b) clay layers in an agglomerate and some intercalated clay layers, and (c) separated single clay layers.

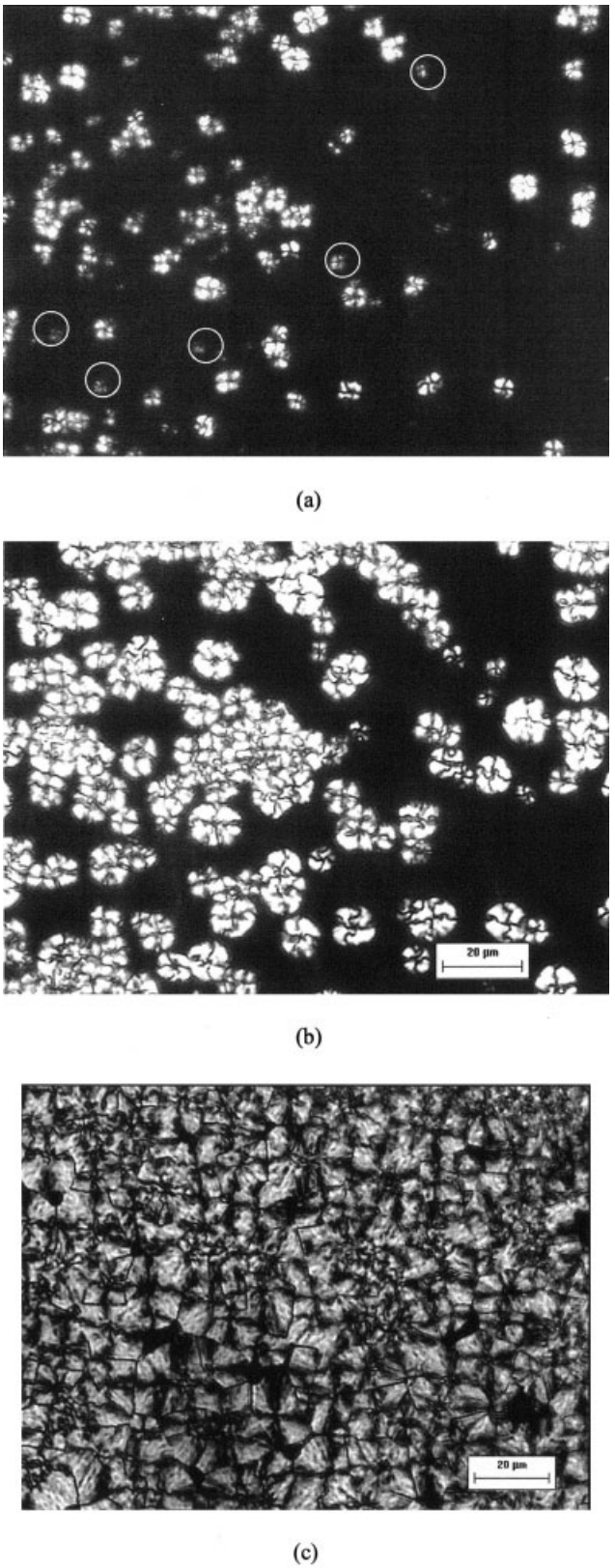

Figure 4 POM pictures of neat PET isothermally crystallized at 226°C, showing (a) spherulites (after 1 min of crystallization), (b) further growth of the spherulites (after 1.5 min of crystallization), and (c) impinged spherulites (after 60 min of crystallization). The circles highlight the spherulitic shape of the small crystallites (bar = 20 μm).

posite. For the raw clay, an intensity maximum occurs at approximately 7.3° (d = 12.1 Å), which corresponds to the basal spacing of the (001) plane of the clay. The modified clay has an intensity maximum at 2θ = 5.2° (d = 17.0 Å). The clay in the PET/clay nanocomposite shows an extremely weak peak around 6.3° 2θ, which implies that the regular clay layer structure may have broken down to some extent in the PET matrix. In addition, when the nanocomposite was heated to 300°C, clay particles could scarcely be observed in the PET matrix with POM, as shown in Figure 2. This indicates that a good dispersion of clay, at least on a submicrometer scale, has been achieved. The fact that clay particles are almost invisible under POM also provides a basis for the study of the matrix crystalline morphology of the nanocomposite with POM.

TEM pictures of the PET/clay nanocomposite are shown in Figure 3. Figure 3(a) shows that clay agglomerates still exist, but in most cases their length is less than 1 μm, and their width is about 100 nm. At a higher magnification, in addition to the agglomerates, both intercalated and exfoliated silicate layers can be observed, as shown in Figure 3(b,c). The PET/clay hybrid synthesized in this work is, therefore, a partially exfoliated nanocomposite, although the extent of exfoliation is not high. Despite its low content and not well exfoliated morphology, the clay has an enormous impact on the crystalline morphology of the PET matrix of this hybrid, which is described in detail in the following sections.

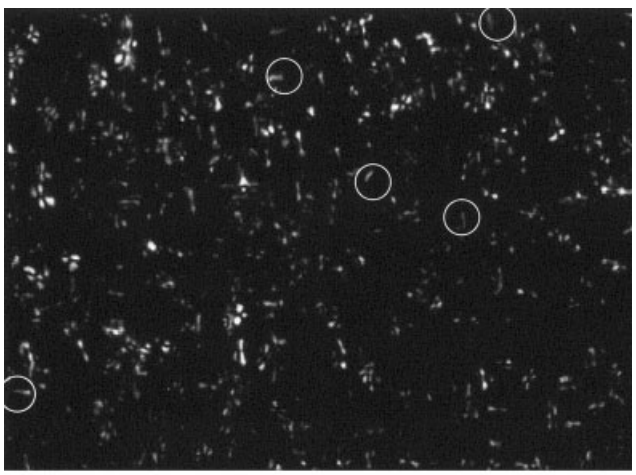

(a)

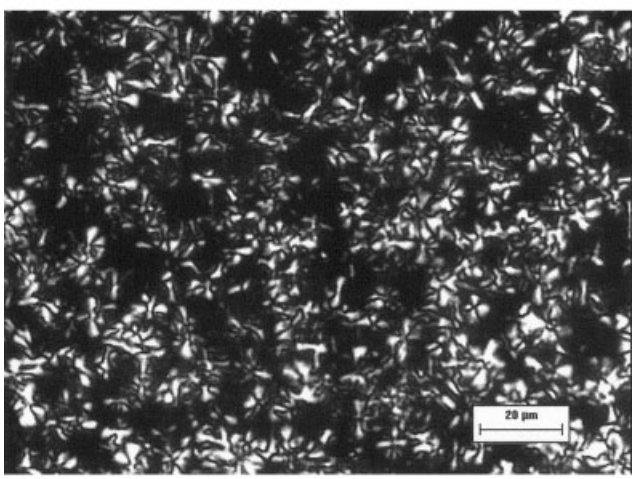

(b)

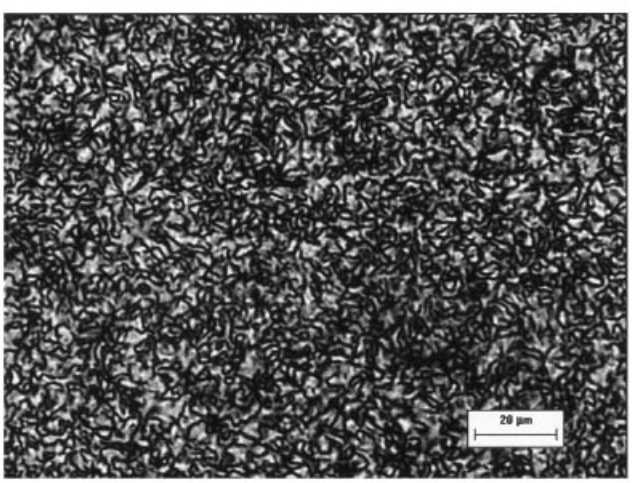

(c)

Crystalline morphology

Polarizing optical micrographs of neat PET and the PET/clay nanocomposite during an isothermal crystallization process at 226°C are shown in Figures 4 and 5, respectively. Figure 4 shows that in neat PET the crystallites have spherulitic superstructures with distinct Maltese cross patterns. The size of the spherulites is fairly uniform, and this indicates dominantly predetermined nucleation. Most of the spherulites grow up to a diameter of about 20 μm. Figure 5 shows that the shape of the crystallites in the PET/clay nanocomposite is very different from that in neat PET. During the initial stage of the crystallization, in addition to spherulites, some small rodlike and irregularly shaped crystallites can be observed, as shown in Figure 4(a). This resembles an observation made for crystallites in a poly(vinyl alcohol)/clay nanocomposite reported by Strawhecker and Manias.[14] After the initial stage, very quickly the rodlike crystallites start to develop more branches in different directions, and gradually they

Figure 5 POM pictures of the PET/clay nanocomposite isothermally crystallized at 226°C, showing (a) rodlike, spherulitic, and irregularly shaped crystallites (after 1 min of crystallization), (b) further growth of the crystallites (after 1.5 min of crystallization), and (c) irregularly shaped crystallites (after 60 min of crystallization). The circles highlight the rodlike shape of some small crystallites (bar = 20 μm).

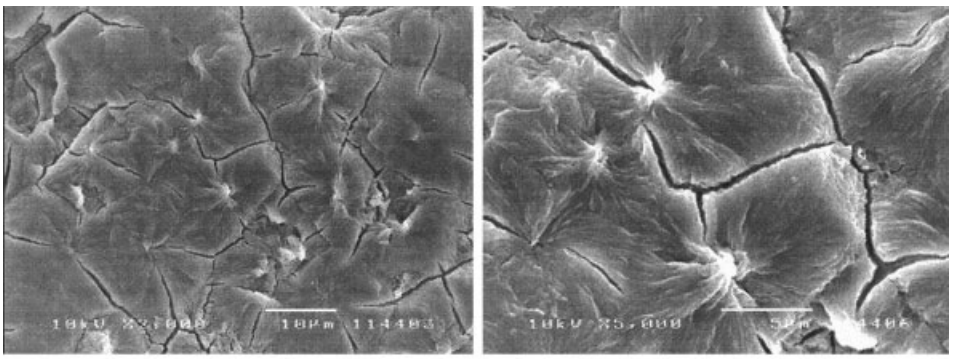

(a) (b)

Figure 6 SEM micrographs of an etched PET sample surface. Before polishing and etching, the sample was isothermally crystallized at 226°C for 30 min.

become irregularly shaped (e.g., fan-shaped crystallites). This implies that the crystal growth becomes three-dimensional in the later stage, whereas in some directions, the crystal growth might be terminated because of the presence of the clay layers. The final size of the irregularly shaped crystallites is less than 5 μm.

SEM micrographs of the etched neat PET and the nanocomposite surfaces are shown in Figures 6 and 7, respectively. Figure 6(a) shows the spherulitic morphology of neat PET; clear boundaries between the spherulites can be observed. The high-magnification micrograph in Figure 6(b) clearly shows the radial texture of the spherulites. Figure 7 shows that the PET/clay nanocomposite does not have a spherulitic morphology. Most of the crystallites are irregularly shaped, and they seem to interlock with each other. The radial texture can be observed at some locations. However, the boundaries between the crystallites are not clear. The absence of clear boundaries between the crystallites implies that the crystal growth is mainly terminated by clay layers rather than impingement. As the polymer chains next to the clay layers are likely to be tethered onto the clay surfaces, a strong interaction may exist between the clay and crystallites that prevents the boundary areas from being etched away. Moreover, the etched surface of the nanocomposite sample is not very smooth because some irregularly shaped amorphous zones have been etched away.

Kinetics of isothermal crystallization

In this study, the following Avrami equation was used in a kinetic analysis of the isothermal crystallization processes:

$$X_c(t) = 1 - \exp(-kt^n) \quad (1)$$

where $X_c(t)$ is the weight fraction of the crystallites at time t, k is the crystallization rate constant, and n is the Avrami exponent. Although an Avrami analysis provides little insight into the structure of the lamellae or spherulites on a molecular level, k and n are very useful diagnostics of the crystallization mechanism.[15]

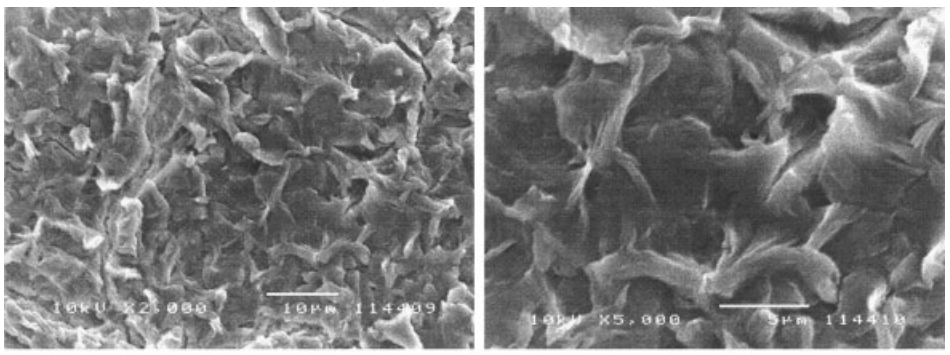

(a) (b)

Figure 7 SEM micrographs of an etched PET/clay nanocomposite sample surface. Before polishing and etching, the sample was isothermally crystallized at 226°C for 30 min.

k includes temperature-dependent terms and contains information regarding diffusion and nucleation rates. n describes crystal growth patterns (one- or two- or three-dimensional) and nucleating mechanisms (predetermined or sporadic).

$X_c(t)$ was calculated with $X_c(t) = A_t/A_\infty$, where A_t is the area of a crystallization peak from $t = 0$ to $t = t$ and A_∞ is the total area of the peak obtained from DSC measurements. Through the plotting of $\ln\{-\ln[1 - X_c(t)]\}$ as a function of $\ln t$, k and n at various crystallization temperatures can be obtained by the fitting of straight lines to the initial parts of the curves. Plots of $\ln\{-\ln[1 - X_c(t)]\}$ versus $\ln t$ for neat PET and the nanocomposite are shown in Figure 8(a,b), respectively.

Figure 9 shows n as a function of the crystallization temperature, which was obtained by the fitting of straight lines to the initial parts of the curves in Figure 8 ($\ln\{-\ln[1 - X_c(t)]\} < -2$). For neat PET, the average n value is about 3, which is in good agreement with previous studies on PET crystallization[16] and also verifies that the crystal growth is three-dimensional (spherulitic) with predetermined nucleation as observed in POM experiments. For the nanocomposite, the average n value is around 2. Furthermore, for neat PET, the n value decreases as the crystallization proceeds, as shown in Figure 8(a), where n corresponds to the slopes of the curves. This phenomenon is typical of most semicrystalline polymers. For the nanocomposite, the curves of $\ln\{-\ln[1 - X_c(t)]\}$ versus $\ln t$ are S-shaped. If we use the points in the range of $\ln\{-\ln[1 - X_c(t)]\} < -2$ to do the calculation, the n value is around 2, whereas if we use the points in the range of $-2 < \ln\{-\ln[1 - X_c(t)]\} < 0$, the n value is around 3. When $\ln\{-\ln[1 - X_c(t)]\}$ is greater than 0, n apparently decreases as $\ln t$ increases, and this is due to secondary crystallization. The Avrami equation is based on the assumption that the radial growth of crystals occurs at a constant rate, and so the impingement of crystals does not occur. As a result, the curves in the range of $\ln\{-\ln[1 - X_c(t)]\} > 0$ should not be used for the determination of Avrami constants.

On the basis of this analysis and the POM and SEM observations, we propose the following crystallization mechanism for the PET/clay nanocomposite. At the crystallization temperature, some polymer chain segments gain relatively straight conformation. If such chain segments are next to a clay surface, they may sit down on it in an ordered manner, which initializes lamellae from the melt in the first place. The lamellae initially may grow one-dimensionally, and when the lamellae grow to a certain stage, their surfaces can act as substrates to initialize more lamellae, and they can

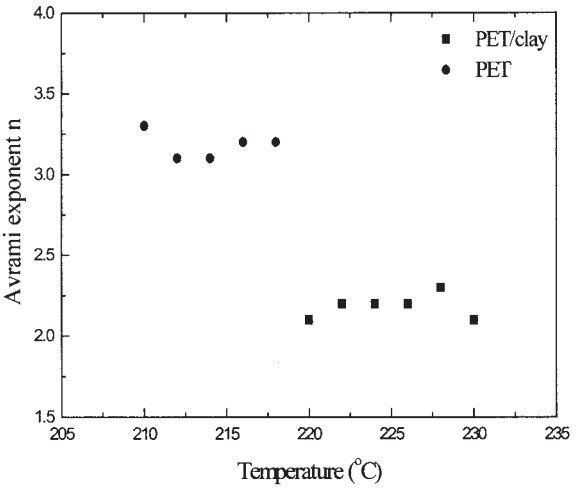

Figure 9 n of neat PET and the PET/clay nanocomposite as a function of the crystallization temperature during the initial stage of the isothermal process ($\ln\{-\ln[1 - X_c(t)]\} < -2$).

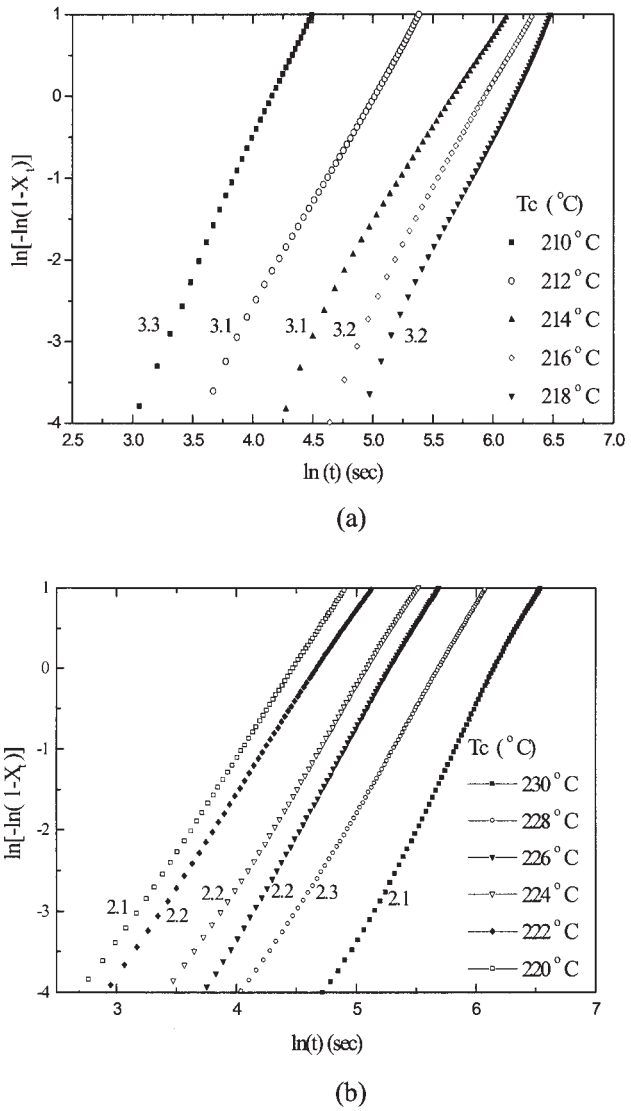

Figure 8 $\ln\{-\ln[1 - X_c(t)]\}$ as a function of $\ln t$ for (a) neat PET and (b) the PET/clay nanocomposite.

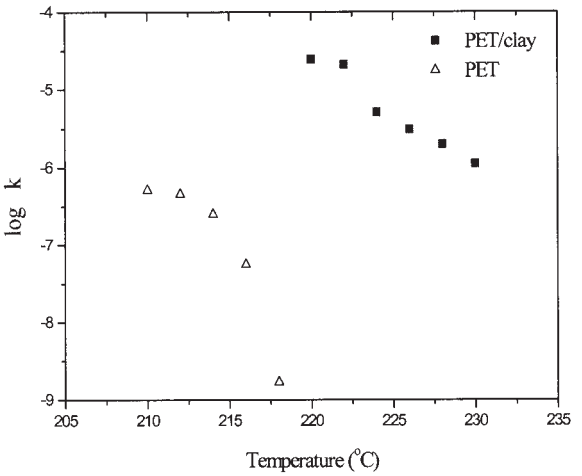

Figure 10 log k of neat PET and the PET/clay nanocomposite as a function of the crystallization temperature during the initial stage of the isothermal process ($\ln\{-\ln[1 - X_c(t)]\} < -2$).

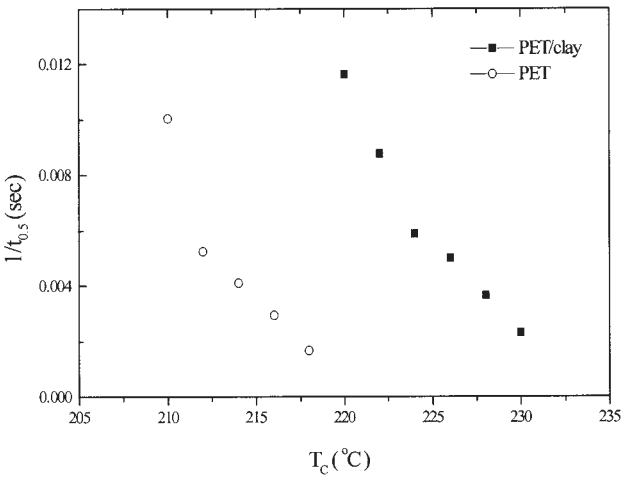

Figure 11 Overall crystallization rate of neat PET and the PET/clay nanocomposite as a function of the crystallization temperature (T_C).

grow three-dimensionally because the nuclei are now not under the geometric constraint imposed by the clay. However, most of the crystallites cannot complete their three-dimensional growth in all directions. Many branches will be terminated because of the presence of the clays in their growth path, and this results in irregularly shaped crystallites interlocked together.

Figure 10 shows k as a function of the crystallization temperature, which was obtained by the fitting of straight lines to the initial parts of the curves ($\ln\{-\ln[1 - X_c(t)]\} < -2$). It indicates that the rate of crystallization of the PET/clay nanocomposite is much higher than that of neat PET at the same temperature. The half-time of crystallization ($t_{0.5}$) was also determined. The dependence of the overall crystallization rate ($1/t_{0.5}$) on the crystallization temperature is plotted in Figure 11. The curves demonstrate that the clay can greatly enhance the overall crystallization rate in the temperature ranges studied. These results coincide with the results reported by Ke and coworkers.[8,9] The greatly increased crystallization rates can be attributed to the heterogeneous nucleating effect of the clay.

Crystalline structure and perfection

To investigate the influence of the clay on the crystalline structure and crystallinity of PET, we performed WAXS experiments on both neat PET and the PET/clay nanocomposite. The results are shown in Figure 12. The diffraction peak positions of the nanocomposite are identical to those of neat PET, and this indicates that the crystal lattice in PET is generally not affected by the presence of clay. From the ratio of the amorphous halo area to the total area, it seems that the crystallinity is also not changed significantly. The (010) and (100) peaks of the nanocomposite are slightly sharper than those of neat PET. This implies that the crystal size in the a and b directions might be slightly larger for the nanocomposite. This finding, however, needs to be verified and explained through further investigation.

To shed light on the lamellar structure of the nanocomposite, we used FTIR to identify trans and gauche conformations of ethylene glycol segments and their relative intensities in neat PET and the PET/clay nanocomposite. In the crystal regions, most of the ethylene glycol segments tend to adopt the trans conformation, whereas in the amorphous region, the ethylene glycol segments may have the gauche conformation, especially in the interfacial region. Figure 13 shows that the bands at 972, 872, and 848 cm^{-1} corresponding to the trans conformation are very clear and

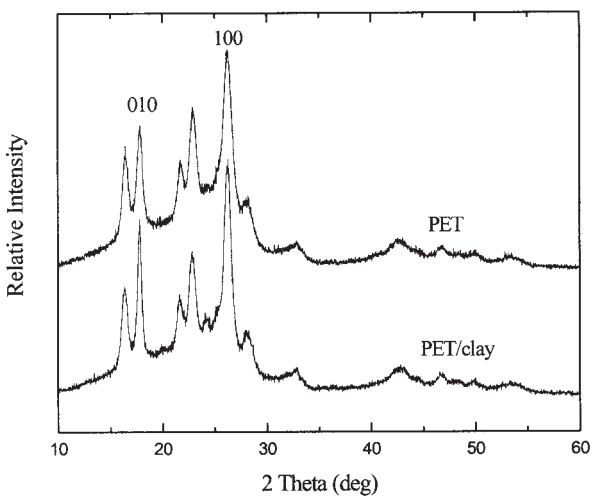

Figure 12 WAXS patterns of neat PET and the PET/clay nanocomposite after isothermal crystallization at 226°C for 1 h.

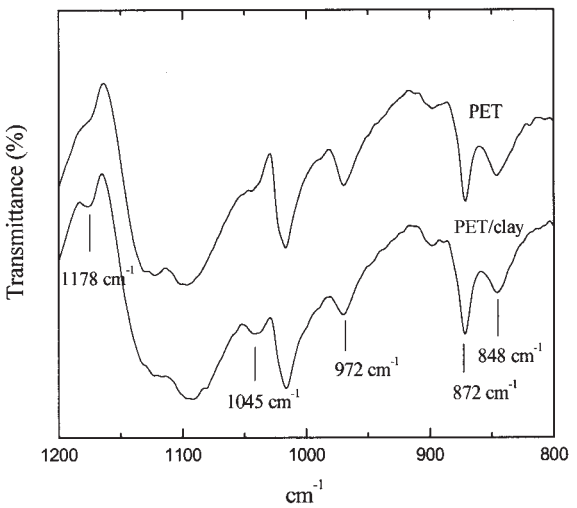

Figure 13 FTIR spectra of neat PET and the PET/clay nanocomposite after isothermal crystallization at 226°C for 1 h.

strong in both neat PET and the nanocomposite. This reveals that both samples have high crystallinity. However, the nanocomposite has significantly stronger gauche bands (1178 and 1045 cm^{-1}) than neat PET. This implies that more ethylene glycol segments may be present in the interfacial region in comparison with neat PET. This may be attributed to the smaller lamellar thickness or the higher degree of imperfection of the crystallites in the nanocomposite with respect to neat PET.

CONCLUSIONS

The crystalline morphology of the PET/clay nanocomposite is very different from that of neat PET. When isothermally crystallized at 226°C, neat PET has a typical spherulitic superstructure with a spherulite size of about 20 μm, whereas some crystallites in the PET/clay nanocomposite are rod-shaped at the beginning and later exhibit three-dimensional growth. The crystallites in the nanocomposite are irregularly shaped, with a size of about 5 μm, and they interlock with each other without clear boundaries. This morphology observation is consistent with the results from the kinetic analysis of the isothermal crystallization process. The WAXS results indicate that the presence of clay does not affect the crystal lattice parameters and crystallinity significantly. An FTIR study has shown that the crystal lamellar thickness or the perfection of the crystals may be reduced because of the presence of clay.

T. Wan and L. Chen thank Nanyang Technological University (Singapore) for postgraduate scholarships.

References

1. Wu, T. M.; Liao, C. S. Macromol Chem Phys 2000, 201, 2820.
2. Lincoln, D. M.; Vaia, R. A.; Wang, Z.; Hsiao, B. S.; Krishnamoorti, R. Polymer 2001, 42, 9975.
3. Liu, X.; Wu, Q. Polymer 2002, 43, 1933.
4. Hambir, S.; Bulakh, N.; Kodgire, P. J Polym Sci Part B: Polym Phys 2001, 39, 446.
5. Xu, W. B.; Liang, G. D.; Zhai, H. B.; Tang, S. P.; Hang, G. P.; Pan, W. P. Eur Polym J 2003, 39, 1467.
6. Tsai, T. Y. In Polymer–Clay Nanocomposites; Pinnavaia, T. J.; Beall, G. W., Eds.; Wiley: New York, 2000; p 173.
7. Davis, C. H.; Mathias, L. J.; Gilman, J. W.; Schiraldi, D. A.; Shields, J. R.; Trulove, P.; Sutto, T. E.; Delong, H. C. J Polym Sci Part B: Polym Phys 2002, 40, 2661.
8. Ke, Y.; Long, C.; Qi, Z. J Appl Polym Sci 1999, 71, 1139.
9. Ke, Y.; Yang, Z. B.; Zhu, C. F. J Appl Polym Sci 2002, 85, 2677.
10. Usuki, A.; Kawasumi, Y.; Okada, A.; Fukushima, Y.; Kamigaito, O. J Mater Res 1993, 8, 1179.
11. Qi, Z.; He, Y.; You, Y. Chin. Pat. CN 1138593A (1998).
12. Kish, M. H.; Borhani, S. J Appl Polym Sci 2000, 78, 1923.
13. Lu, X. F.; Hay, J. N. Polymer 2001, 42, 8055.
14. Strawhecker, K. E.; Manias, E. Macromolecules 2001, 34, 8475.
15. Hay, J. N. Br Polym J 1971, 3, 74.
16. Kim, S. H.; Park, S. W.; Gil, E. S. J Appl Polym Sci 1998, 67, 1383.